Energy & Environmental Science

Cite this: *Energy Environ. Sci.*, 2012, **5**, 8351

www.rsc.org/ees

PAPER

Thermopower enhancement in conducting polymer nanocomposites *via* carrier energy scattering at the organic–inorganic semiconductor interface†

Ming He,[a] Jing Ge,[a] Zhiqun Lin,[b] Xuhui Feng,[c] Xinwei Wang,[c] Hongbin Lu,[a] Yuliang Yang[a] and Feng Qiu*[a]

Received 30th March 2012, Accepted 14th June 2012
DOI: 10.1039/c2ee21803h

The energy-filtering effect was successfully employed at the organic–inorganic semiconductor interface of poly(3-hexylthiophene) (P3HT) nanocomposites with the addition of Bi_2Te_3 nanowires, where low-energy carriers were strongly scattered by the appropriately engineered potential barrier of the P3HT–Bi_2Te_3 interface. The resulting P3HT–Bi_2Te_3 nanocomposites exhibited a high power factor of 13.6 μW K^{-2} m^{-1} compared to that of 3.9 μW K^{-2} m^{-1} in P3HT. The transport characteristics of nanocomposites, including the carrier concentration, mobility, and energy-dependent scattering parameter, were revealed by the experimental measurements of electrical conductivity, Seebeck coefficient, and Hall coefficient to quantitatively elucidate the carrier energy scattering at the P3HT–Bi_2Te_3 interface. The ability to rationally engineer the organic–inorganic semiconductor interfaces of polymer nanocomposites to achieve an improved Seebeck coefficient and power factor provides a potential route to high-performance, large-area, and flexible polymer thermoelectric materials.

1. Introduction

The direct conversion between heat and electricity in thermoelectric (TE) materials offers a promising route towards the development of power generation and refrigeration without moving parts.[1] The energy conversion efficiency of these simple, automatic and eco-friendly TE devices is quantified by the materials' dimensionless figure-of-merit $ZT = \sigma\alpha^2 T/\kappa$, where σ is the electrical conductivity, α is the Seebeck coefficient (also called the thermopower), κ is the thermal conductivity and T is the absolute temperature. The power factor P is calculated from the measured electrical conductivity and Seebeck coefficient where $P = \sigma\alpha^2$. A high-performance TE material requires a low thermal conductivity to prevent thermal shorting, a high electrical conductivity to reduce Joule heating and a high Seebeck coefficient to promote the energy conversion of heat to electricity or electricity to cooling.[2] However, the strong interdependence of these three parameters (*i.e.*, increasing σ is usually accompanied

[a]*State Key Laboratory of Molecular Engineering of Polymers, Department of Macromolecular Science, Fudan University, Shanghai, 200433, China. E-mail: fengqiu@fudan.edu.cn*
[b]*School of Materials Science and Engineering, Georgia Institute of Technology, Atlanta, GA, 30332, USA*
[c]*Department of Mechanical Engineering, Iowa State University, Ames, Iowa 50011, USA*

† Electronic supplementary information (ESI) available: The measurement of Seebeck coefficient, the electrical conductivity and Seebeck coefficient of P3HT at different doping levels, and the detailed calculation of transport parameters. See DOI: 10.1039/c2ee21803h

Broader context

Thermoelectric (TE) materials have attracted great attention as a simple, automatic and eco-friendly means of energy conversion owing to their unique capability to directly convert heat to electricity. The performance of TE materials depends on the figure-of-merit ZT, which has been significantly promoted in nanostructured inorganics *via* band engineering, phonon scattering, energy-barrier filtering, *etc.* We demonstrate here that the strategy of rationally engineering semiconductor interfaces to enhance the ZT can also be employed in polymer-based TE materials, where low-energy carriers are strongly scattered by the potential barrier of the organic–inorganic semiconductor interface leading to a remarkable increased power factor. The transport characteristics of nanocomposites, including the carrier concentration, mobility, and energy-dependent scattering parameter, are revealed by the experimental measurements of electrical conductivity, Seebeck coefficient, and Hall coefficient to quantitatively elucidate the carrier energy scattering at the organic–inorganic semiconductor interface. These polymer-based TE materials will also capitalize on the advantages peculiar to polymers, such as low cost, processability, flexibility, light weight, roll-to-roll production and large area, which coincide well with the requirements of the near-future market in electronics that move toward personal, portable, and polymer-based flexible electronics.

by an increased κ and a decreased α) imposes restrictions on maximizing ZT in homogeneous bulk materials.[3] Recently, significant improvements on ZT have been achieved in nanostructured inorganics (*e.g.*, superlattices, nanoinclusions, nanocomposites, *etc.*),[4–7] in particular, by phonon scattering to preferentially reduce the thermal conductivity without the loss of power factor,[4] and by energy filtering to independently promote the Seebeck coefficient without greatly suppressing electrical conductivity.[7] However, these complex inorganic nanostructures are generally prepared by either the ball-milling, melt-spinning method or molecular beam epitaxy, which involves high-temperature, long-term and high-cost fabrication processes.[8]

In this context, considerable efforts have been made to develop a facile and low-cost fabrication process for nanostructured TE materials, including wet-chemical synthesis,[9] solution-processable nanocomposites,[8] and polymer TE materials.[10] Quite intriguingly, the strategy of introducing nanostructured interfaces to scatter phonons or filter low-energy carriers seems to also work well in polymer TE materials. Although based on qualitative interpretations, the improved Seebeck coefficients in polyaniline/carbon nanotube (CNT) and poly(3,4-ethylenedioxythiophene)–tellurium nanocomposites were reported and ascribed to the possibility of an energy-filtering effect.[11,12] Inspired by these precursory results, we focused on rationally engineering the organic–inorganic semiconductor interfaces of polymer nanocomposites to improve the Seebeck coefficient and power factor *via* the energy-filtering effect. The organic–inorganic interface was created by mixing inorganic nanoparticles into a polymer matrix through a solution-processable route. Several important rules for constructing the energy-filtering interface were adopted: (1) intimate contacts between polymer and nanoparticles to establish clear organic–inorganic interfaces, (2) similar work functions of polymer and nanoparticles to facilitate high-energy carriers transferring across the interfaces, (3) an interfacial barrier height of below 100 meV to selectively scatter low-energy carriers rather than high-energy carriers, (4) one-dimensional nanostructures to build effective potential barriers in a low filler concentration compared to that of zero-dimensional nanoparticles.[11–14] It is noteworthy that the energy-filtering approach was originally proposed for superlattices where alternate energy barrier layers could act as energy filters; it has been recently extended to three-dimensional bulk inorganics where either nanoparticles or grain boundary interfaces play the role as an energy filter.[14] In this study, we demonstrated that the organic–inorganic semiconductor interface of conducting polymer nanocomposites could also act as an energy filter to substantially scatter low-energy carriers, which could be verified by the increased energy-dependent scattering parameter in nanocomposites.

Compared to inorganics, conducting polymers possess an intrinsically low thermal conductivity (*i.e.*, 0.1–2 W K^{-1} m^{-1}), thereby providing unique opportunities to exploit them for the development of next-generation organic TE materials.[15] These organic TE materials capitalize on the advantages peculiar to polymers, such as low cost, processability, flexibility, light weight, roll-to-roll production and large area,[16] which coincide well with the requirements of the near-future market in electronics that move toward personal, portable, and polymer-based flexible electronics.[17] Among various conducting polymers, poly(3-hexylthiophene) (P3HT) is one of the most widely studied organic semiconductors and possesses excellent solution processability, chemical stability and high field-effect mobility.[18–22] The electrical conductivity of P3HT ($10^{-8} \sim 10^{5}$ S m^{-1}) depends largely on the level of doping with suitable dopants (*e.g.*, $FeCl_3$, I_2, $HClO_4$, *etc.*).[23] In addition, the band structure of polythiophene in varied doping levels has been systematically studied by both experimental measurement and theory calculation.[24] As a state-of-the-art inorganic TE material at room temperature, Bi_2Te_3 exhibits high ZT values in both bulk solids (*i.e.*, ZT $\approx$ 0.5) and nanostructured alloys (*i.e.*, ZT $\approx$ 1.04 for n-type $BiTe_{3-y}Se_y$ and 1.4–1.6 for p-type $Bi_xSb_{2-x}Te$).[25] Because the work function of Bi_2Te_3 (*i.e.*, ~5.3 eV) is larger than that of P3HT (*i.e.*, ~4.1 eV),[26,27] the charge carriers can readily transfer from P3HT to Bi_2Te_3 in the absence of the potential barrier yielded by the work-function difference. Therefore, the height of the interfacial potential barrier is probably determined by the band-aligning levels of P3HT and Bi_2Te_3.[28] The band gap of Bi_2Te_3 is about 0.16 eV,[29] and the band gap of P3HT relies on the doping level (*i.e.*, ranging from ~2.0 eV to < 0.1 eV).[24] As a result, the potential barrier of the P3HT–Bi_2Te_3 interface can possibly be engineered by adjusting the doping level of P3HT,[30] leading to an optimized carrier scattering at the P3HT–Bi_2Te_3 interface, and thus the enhancement of TE performance.

Herein, we report a remarkable enhancement in the Seebeck coefficient and power factor of P3HT by mixing with Bi_2Te_3 nanowires to substantially scatter low-energy carriers *via* the energy-filtering effect at the P3HT–Bi_2Te_3 interface. With a template-free synthesis of Bi_2Te_3 nanowires and a solution-processable fabrication of nanocomposites, the resulting P3HT–Bi_2Te_3 nanocomposites exhibited a high power factor of 13.6 μW K^{-2} m^{-1}. The effects of the weight ratio of Bi_2Te_3 nanowires and the doping level of P3HT on the TE performance were systematically studied. The transport characteristics of P3HT–Bi_2Te_3 nanocomposites were further explored by deriving the carrier concentration, mobility and energy-dependent scattering parameter from the experimental measurements of electrical conductivity, Seebeck coefficient and Hall coefficient in order to quantitatively elucidate the carrier energy scattering at the P3HT–Bi_2Te_3 interface.

2. Experimental section

2.1 Materials

Regioregular P3HT (M_n = 19 000 g mol^{-1}, PDI = 1.2, regioregularity > 98%) was synthesized by a modified Grignard metathesis procedure, and the detailed synthesis procedure can be found in our previous work.[20,22] Chloroform, Na_2TeO_3, $BiCl_3$, $N_2H_4 \cdot H_2O$, ethylene glycol and anhydrous-$FeCl_3$ were purchased from Sigma-Aldrich.

2.2 Bi_2Te_3-nanowire synthesis

Bi_2Te_3 nanowires were synthesized through a modified template-free reaction,[31] by adding Bi precursors to the as-synthesized Te in an ethylene glycol solution, resulting in the formation of Bi_2Te_3 nanowires. In general, Na_2TeO_3 (0.116 g, 0.52 mmol) and $BiCl_3$ (0.110 g, 0.35 mmol) were completely dissolved in 20 ml ethylene glycol, respectively, by stirring at 150 °C for 10 min to

get clear Te- and Bi-precursor solutions. The molar ratio of $BiCl_3$ to Na_2TeO_3 was nearly 2 : 3. $N_2H_4 \cdot H_2O$ (1 ml, 64–65 % in water) was then injected into the Te- precursor solution, and the solution quickly turned from colorless to grey. Two minutes later, the Bi-precursor solution was injected into the grey mixture and the solution turned from grey to black within 2 min. The black solution was stirred at 150 °C for 5 min and cooled to room temperature. The black precipitates were washed with acetone for 5 times and dried in a vacuum oven at 70 °C overnight.

2.3 Sample preparation

P3HT was doped with anhydrous $FeCl_3$ in $CHCl_3$ by stirring at 40 °C for 12 h, and varied weight ratios of Bi_2Te_3 nanowires (*i.e.*, 5 wt%, 10 wt%, 15 wt% and 20 wt%) were added into the $FeCl_3$-doped P3HT solution, respectively. The P3HT–Bi_2Te_3 mixture was thoroughly mixed by ultrasonication at 40 °C for 30 min, and drop-cast onto a 24 × 24 mm^2 glass slide which was pre-cleaned sequentially by ultrasonication in acetone, hexane and deionized-water. The drop-cast solution was rapidly dried in a vacuum oven at room temperature to form a uniform P3HT–Bi_2Te_3 nanocomposite film; the film thickness was 15 ± 2 μm. The pure $FeCl_3$-doped P3HT film without Bi_2Te_3 was also prepared in the same way.

2.4 Characterization

X-ray diffraction (XRD) data were collected by a PANalytical X'Pert PRO X-ray diffractometer using Cu Kα_1 radiation (λ = 1.541 Å) operating at 40 kV and 40 mA. Transmission electron microscopy (TEM) imaging was performed on a FEI Tecnai G2-20 transmission electron microscope at an accelerating voltage of 200 kV. Scanning Electron Microscope (SEM) imaging was carried out on a Tescan TS-5136MM scanning electron microscope operating at 20 KV. Thermal conductivity was measured by the transient electrothermal technique (see details in the ESI†).[32] Electrical conductivity was measured by the standard four-probe method using a Four-Probe Tech RTS-4 electrical conductivity measurement system. The Seebeck coefficient was obtained by measuring the electrical potential difference when a temperature gradient was established between two ends of the nanocomposite film. The Seebeck coefficient of Pt at room temperature was measured as a reference sample, and the measured value of 5.3 ± 0.1 μV K^{-1} was in good agreement with the literature value of 5.2 μV K^{-1} (see Fig. S1 in the ESI†). The Hall coefficient was measured by an Ecopia HMS3000 Hall effect measurement system with a magnetic field of 0.550 T and an electric current of 1 mA with a good Ohm contact established using Au electrodes.

3. Results and discussion

3.1 Preparation of P3HT–Bi_2Te_3 nanocomposites

Bi_2Te_3 nanowires were synthesized by a modified template-free reaction between sodium tellurite and bismuth chloride in the presence of hydrazine hydrate and ethylene glycol (see Experimental section).[31] It is well known that ethylene glycol is a versatile solvent for controlling the oriented crystallization and stabilization of one-dimensional inorganic nanostructures.[33,34] The uniform one-dimensional tellurium nanostructures could be synthesized, dispersed in ethylene glycol, and used as templates to generate more complex nanostructured materials.[31] Our synthesis method is similar to the hydrothermal synthesis of Bi_2Te_3 nanowires through the solid-state interdiffusion of Bi and Te atoms by the hydrothermal method,[35] wherein polycrystalline Bi_2Te_3 nanowires were prepared by the nucleation of Bi atoms on the surface of Te nanowires which were previously synthesized in ethylene glycol to serve as templates. Fig. 1a and b show representative TEM images of nearly uniform-sized Bi_2Te_3 nanowires formed by injecting the Bi-precursor solution into the Te-nanowire dispersion solution. The length of the nanowires is around 5–10 μm. The width is about 50–200 nm, which is close to that of Bi_2Te_3 nanowires/nanotubes prepared by hydrothermal synthesis and electrochemical deposition.[36] The XRD pattern of as-synthesized Bi_2Te_3 nanowires after the removal of ethylene glycol by repeatedly washing in acetone is shown in Fig. 1c. All the diffraction peaks are readily indexed to a rhombohedral structure (JCPDS 01-82-0358) with lattice constant of a = 4.40 Å and c = 30.44 Å, and no impure diffraction peak is observed, suggesting that only a single phase of well-crystallized Bi_2Te_3 existed in the final product. We note that the molar ratio of 2 : 3 between the Bi and Te precursors is crucial for obtaining a single phase of Bi_2Te_3 and the reaction temperature of 150 °C is preferred for the oriented growth of Bi_2Te_3 into one-dimensional nanowires.

Subsequently, Bi_2Te_3 nanowires were thoroughly mixed with a $FeCl_3$-doped P3HT chloroform solution, followed by rapidly drying under vacuum to obtain a uniform nanocomposite film. Our template-free synthetic method of Bi_2Te_3 nanowires

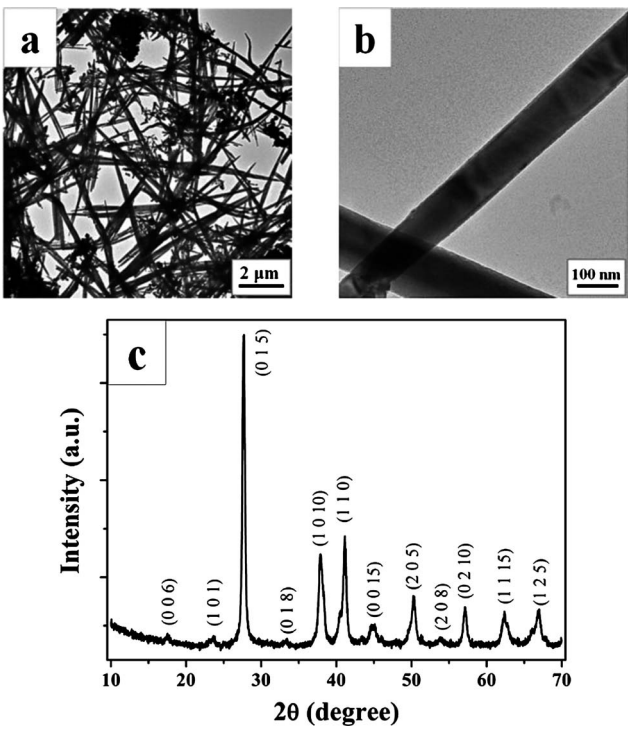

Fig. 1 (a and b) Representative TEM images of Bi_2Te_3 nanowires synthesized by the template-free method in ethylene glycol; (c) XRD pattern of the synthesized Bi_2Te_3 nanowires, in which the peaks are readily indexed to the standard profile of JCPDS 01-82-0358.

dispensed with the need for the ligand-exchange approach as in previous studies (*i.e.*, remove insulating organic ligands that would otherwise hinder electronic interaction and cause phase separation between organic–inorganic blends) and enabled the direct contact between P3HT and Bi_2Te_3.[37] Fig. 2 shows representative SEM images of P3HT and P3HT–Bi_2Te_3 nanocomposite films, which reveal that Bi_2Te_3 nanowires were homogeneously dispersed within the P3HT matrix (*i.e.*, 10 wt% Bi_2Te_3 in Fig. 2b and 20 wt% Bi_2Te_3 in Fig. 2c), and no microphase separation between P3HT and Bi_2Te_3 nanowires was observed (Fig. S2 in the ESI†). All of the P3HT mentioned in the context was doped with $FeCl_3$ unless specially noted (see Experimental section). Clearly, Bi_2Te_3 nanowires near to the top surface of the nanocomposite film appeared bright while the P3HT matrix appeared grey or dark in the SEM images (Fig. 2b and c) because of the higher electron density of inorganic nanowires than that of P3HT.[37] However, for the Bi_2Te_3 nanowire embedded inside the nanocomposite film, it appeared light grey or difficult to see.

3.2 Thermoelectric characteristics of P3HT–Bi_2Te_3

The thermal conductivity of as-prepared P3HT–Bi_2Te_3 films at room temperature was measured using the transient electrothermal technique.[32] The weight ratio of Bi_2Te_3 nanowires in the nanocomposites varied from 5 wt% to 20 wt%. The P3HT matrix (*i.e.*, with 0 wt% Bi_2Te_3) was heavily doped by $FeCl_3$ to attain a high electrical conductivity. As shown in Fig. 3a, the heavily doped P3HT matrix (*i.e.*, 32 wt% $FeCl_3$, σ = 1800 S m^{-1}) exhibited a relatively low thermal conductivity of ~0.54 W K^{-1} m^{-1}, comparable to the value measured using the 3ω-technique (*i.e.*, ~0.48 W K^{-1} m^{-1}).[38] It is noteworthy that the thermal conductivity of heavily doped P3HT was only slightly higher than that of pristine P3HT (*i.e.*, ~0.2 W K^{-1} m^{-1}) and close to

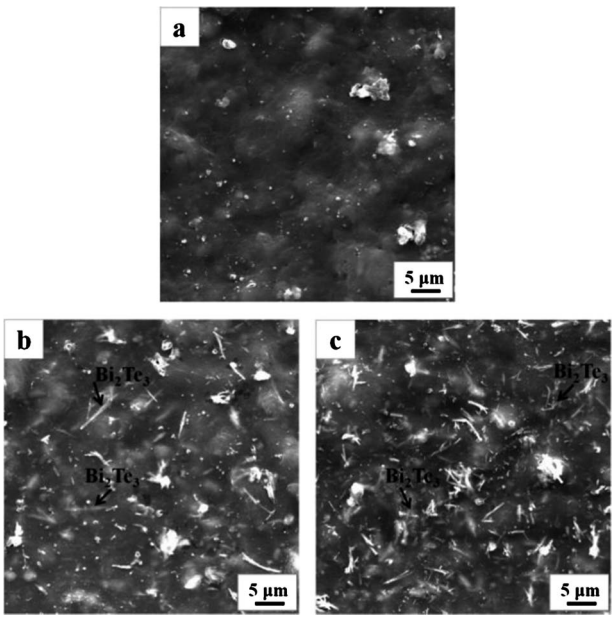

Fig. 2 Representative SEM images of P3HT and P3HT–Bi_2Te_3 films: (a) $FeCl_3$-doped P3HT solely; (b) $FeCl_3$-doped P3HT with 10 wt% Bi_2Te_3 nanowires; (c) $FeCl_3$-doped P3HT with 20 wt% Bi_2Te_3 nanowires.

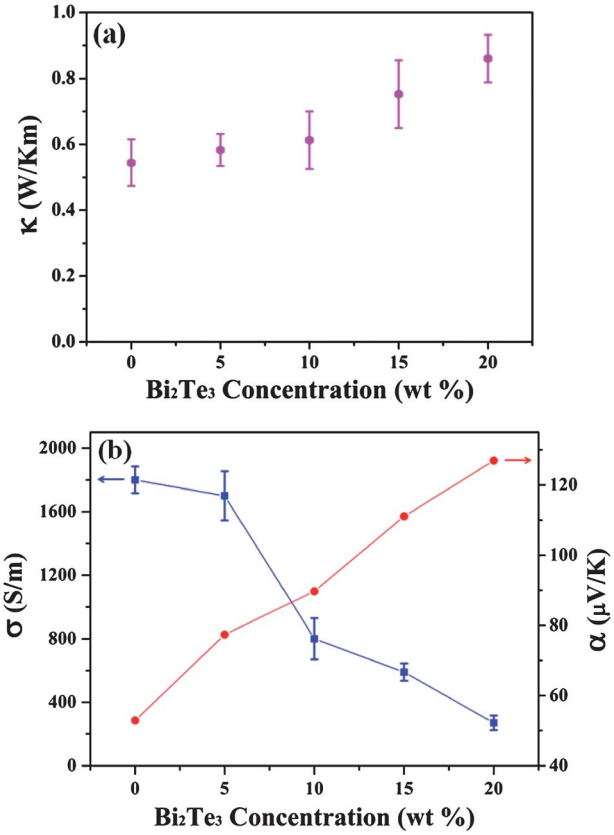

Fig. 3 (a) Thermal conductivity of P3HT–Bi_2Te_3 nanocomposites at room temperature; (b) the electrical conductivity and Seebeck coefficient as a function of the weight ratio of Bi_2Te_3 nanowires in the P3HT–Bi_2Te_3 nanocomposites. The doping level of the P3HT matrix was about 32 wt% and the weight ratio of Bi_2Te_3 nanowires varied from 0 wt% to 20 wt%.

that of lightly or moderately doped P3HT.[15] Although a further increase in the thermal conductivity was then observed with the addition of Bi_2Te_3 nanowires in the matrix, the conductivity value remained at a very low level even at the highest Bi_2Te_3 concentration (*i.e.*, ~0.86 W K^{-1} m^{-1} with 20 wt% Bi_2Te_3). Similar results have been reported in polymer–CNT nanocomposites; their low thermal conductivity was ascribed primarily to the high interface density (*i.e.*, the interfacial area per unit volume) between polymer and CNTs,[11] because the reduction of thermal conductivity was dominated by the phonon-interface scattering, and a high interface density could scatter phonons more effectively, resulting in a lower thermal conductivity.[39] This distinctive feature of low thermal conductivity in conducting polymer nanocomposites promotes the exploitation of high-performance polymer TE materials and thus allows for the attempts to enhance the power factor.

The electrical conductivity and Seebeck coefficient of the prepared P3HT–Bi_2Te_3 films were then measured by the standard methods (see Experimental section). Shown in Fig. 3b are the representative electrical conductivity and Seebeck coefficient as a function of the weight ratio of Bi_2Te_3 nanowires in the nanocomposites. It is clear that a higher weight ratio of Bi_2Te_3 nanowires gives a higher Seebeck coefficient but a lower electrical conductivity in nanocomposites. Similar trends were observed in the Seebeck coefficient and electrical conductivity of the P3HT

matrix measured as a function of the doping level (see Fig. S3 in the ESI†). The power factor of 24 wt% $FeCl_3$-doped P3HT was 3.9 μW K^{-2} m^{-1}, which is consistent with previously reported work that the power factor of doped P3HT usually reached a maximum at 20–30% doping, depending on the balance between electrical conductivity and Seebeck coefficient.[40] For conducting polymers, the electrical conductivity originates from the existence of charge carriers introduced by doping and the phonon-assisted hopping of charge carriers along the polymer chains,[24] so a high doping level leads to a high carrier concentration, large charge mobility and thus good electrical conductivity. On the other hand, the increase of carrier concentration in the electronic structure of conducting polymers reduces the energy gap between the average electron energy and the Fermi level, which in turn leads to the decrease of the Seebeck coefficient.[15,41]

Fig. 4a shows the correlation between the Seebeck coefficient and electrical conductivity in both P3HT and P3HT–Bi_2Te_3 nanocomposites. For P3HT films, the electrical conductivity was delicately tailored by changing the $FeCl_3$-doping level from 1 wt% to 32 wt%, the resulting electrical conductivity of the films varied from ~3 S m^{-1} to ~1800 S m^{-1}. For the nanocomposite films, a series of Bi_2Te_3 nanowires (*i.e.*, 5 wt%, 10 wt%, 15 wt% and 20 wt%) were mixed with the P3HT matrix at different doping levels (*i.e.*, 8 wt%, 16 wt%, 24 wt% and 32 wt%, respectively); the resulting electrical conductivity of the nanocomposite films varied from ~2 S m^{-1} to ~1700 S m^{-1}. Both the Seebeck coefficients of P3HT and P3HT–Bi_2Te_3 progressively decreased from 450 μV K^{-1} to below 100 μV K^{-1} with the increased electrical conductivity, which is due primarily to the increased carrier concentration introduced by doping as discussed above.[15,41] Quite intriguingly, in the range of high electrical conductivity (*i.e.*, $\sigma > 200$ S m^{-1}, Fig. 4a), P3HT–Bi_2Te_3 nanocomposites exhibited higher Seebeck coefficients than the P3HT films, thereby leading to markedly improved power factors in the nanocomposites in comparison to those of P3HT films (Fig. 4b). Compared to that of 3.9 μW K^{-2} m^{-1} in P3HT films, a high power factor of 13.6 μW K^{-2} m^{-1} at room temperature was attained in P3HT–Bi_2Te_3 nanocomposites, implying that the power factor of conducting polymers could be effectively enhanced by the incorporation of semiconductor nanowires. It is worth noting that the enhancement of the Seebeck coefficient and power factor in P3HT–Bi_2Te_3 nanocomposites did not appear in the range of low electrical conductivity (*i.e.*, $\sigma < 200$ S m^{-1}, the inset of Fig. 4a), where the Seebeck coefficient and power factor were slightly lower than those of P3HT, indicating that the improved TE property in P3HT–Bi_2Te_3 nanocomposites was not simply associated with the physical mixing of Bi_2Te_3. The enhanced power factor was also not observed in the nanocomposites of P3HT and Bi_2Te_3 nanoparticles (data not shown), suggesting that the one-dimensional morphology of Bi_2Te_3 nanowires played an important role in the enhancement of thermoelectric performance. It was predicted that nanoparticles would need a much higher concentration than nanowires to form an effective energy filter in nanocomposites, because even low-energy electron wave functions can go round the nanoparticle.[14]

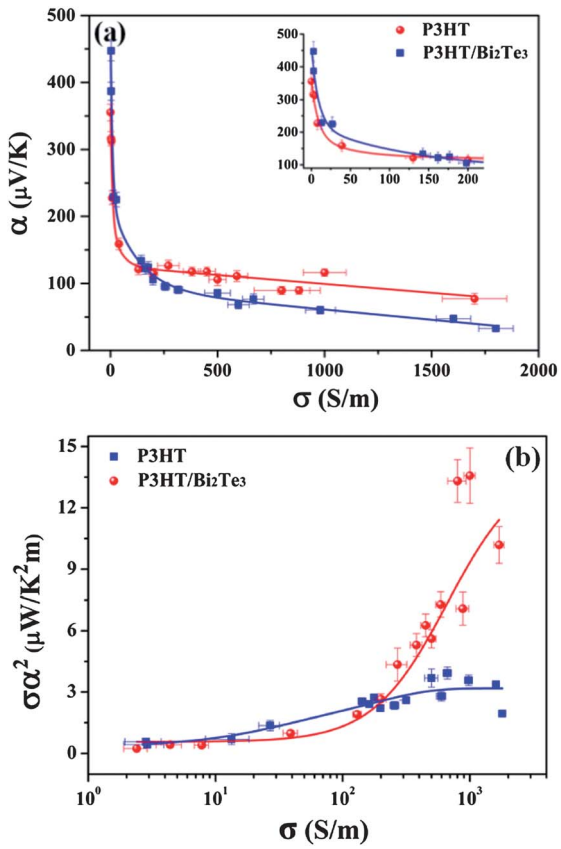

Fig. 4 (a) The correlation between the Seebeck coefficient α and the electrical conductivity σ in P3HT and P3HT–Bi_2Te_3 nanocomposites; the inset shows the close-up in the range of low electrical conductivity (*i.e.*, $\sigma < 200$ S m^{-1}); (b) the correlation between the power factor $\sigma\alpha^2$ and the electrical conductivity σ in P3HT and P3HT–Bi_2Te_3 nanocomposites.

3.3 Transport characteristics of P3HT–Bi_2Te_3

It is of key importance to understand the origin of the enhanced Seebeck coefficient and power factor in P3HT by the mixing of Bi_2Te_3 nanowires. To this end, we turn our attention to quantitative elucidation of the energy-filtering effect in the P3HT–Bi_2Te_3 nanocomposite by investigating its transport characteristics. The positive sign of the Seebeck coefficients in both P3HT and P3HT–Bi_2Te_3 (Fig. 4a) was related to the p-type character of the semiconductor. By taking the relaxation-time approximation,[7] the experimentally measured electrical conductivity, Seebeck coefficient and Hall coefficient (see Experimental section) can be described by the function of a series of characterization transport parameters, namely, the Fermi level E_f, band gap E_g, effective mass m^*, carrier concentration n, and energy-dependent scattering parameter λ (see eqn (S9)–(S11) in the ESI†).[14] For the heavily doped P3HT matrix (*i.e.*, 24 wt% $FeCl_3$ doping), the band gap E_g was estimated to be 0.2 eV,[30,42,43] the effective mass m^* was assumed to be $1.7m_e$ (*i.e.*, m_e is the free electron mass),[44,45] and the other transport parameters (*i.e.*, E_f, n and λ) could thus be derived by numerically solving the integral non-linear equations of S9–S11 (see details in the ESI†). Similarly, the transport parameters of the P3HT–Bi_2Te_3 nanocomposite (*i.e.*, 20 wt% Bi_2Te_3 nanowires mixed in 24 wt% $FeCl_3$-doping P3HT) could also be calculated using E_g and m^* of the P3HT matrix, as the Bi_2Te_3 concentration was below the percolation threshold (*i.e.*, Bi_2Te_3-nanowire concentration >40 wt%, where Bi_2Te_3 nanowires form

effective electrical interconnects in the nanocomposite); the charge carrier transport of the nanocomposite was, in principle, dominated by that of the P3HT host matrix.[28] The measured values and calculated results are all summarized in Table 1. It is noteworthy that the calculated Fermi level of the P3HT matrix (*i.e.*, $E_f \approx -0.7$ eV) agreed well with previously reported work,[30,46] which is indicative of the validity of the calculation method. Moreover, when substituting these calculated parameters into eqn (S10) and (S11) (see ESI†), the calculated Seebeck coefficient and Hall coefficient were in good agreement with the experimentally measured values (*i.e.*, error <10%).

As shown in Table 1, compared to the P3HT matrix, the P3HT–Bi_2Te_3 nanocomposite typically exerted a 5-fold increase in the Seebeck coefficient with a slight, 2-fold decrease in the electrical conductivity, as a result of which a significant 12-fold enhancement in the power factor was reached. The enhanced Seebeck coefficient can be attributed to the large scattering parameter in the nanocomposite, as the carrier concentration of P3HT–Bi_2Te_3 was nearly the same as that of P3HT. The increased scattering parameter (*i.e.*, $\lambda = 2.99$ in the composite compared to $\lambda = 1.13$ in the host matrix) provided solid evidence for the energy-filtering effect at the P3HT–Bi_2Te_3 interface, in conjugation with the enhanced Seebeck coefficient and power factor. In particular, for the P3HT–Bi_2Te_3 nanocomposite, low-energy carriers were strongly scattered by the potential barrier at the P3HT–Bi_2Te_3 interface with the addition of Bi_2Te_3 nanowires in the P3HT matrix, and only high-energy carriers could effectively transfer across the interface.[14] Actually, high-energy carriers were able to transfer more heat than low-energy carriers, resulting in the increase of the Seebeck coefficient.[3] The modelling method was further applied to extract the Fermi energy, scattering parameter, carrier concentration and mobility of the nanocomposites as a function of Bi_2Te_3 concentration, which varied from 5 wt% to 20 wt%. All the results are listed in Table S1 in the ESI†. It can be found that: (1) the Fermi energy of each group is nearly consistent (*i.e.*, ~0.7 eV); (2) the scattering parameter increased from 1.1 to 3.0 when the Bi_2Te_3 concentration reached ≥10 wt%, suggesting that no specific effect with the loading concentration of Bi_2Te_3 on the carrier energy scattering was present (Table S1 and S2 in the ESI†); (3) the carrier concentration and mobility decreased with the addition of Bi_2Te_3 nanowires. Considering that the energy-scattering interface can also simultaneously reduce the carrier mobility μ, it is not surprising that the carrier mobility in the composite was lower than that of the P3HT matrix. Hence, the design of a potential barrier at the organic–inorganic semiconductor interface must balance the Seebeck coefficient and carrier mobility in order to yield a maximized power factor, which essentially depends on the height of interfacial potential barrier. The optimized barrier height was suggested to be less than 100 meV according to the theoretical calculation.[13]

Table 1 Summary of the transport parameters of the P3HT and P3HT–Bi_2Te_3 nanocomposites. The doping level of the P3HT matrix was about 24 wt%, and the P3HT–Bi_2Te_3 nanocomposite was prepared by mixing 20 wt% Bi_2Te_3 nanowires in the P3HT matrix. The electrical conductivity, Seebeck coefficient and Hall coefficient were experimentally measured by the standard methods (see Experimental section), and the other parameters were derived from the measured values (see ESI†)

Transport parameters	P3HT	P3HT–Bi_2Te_3
Electrical conductivity σ (S m^{-1})	930	450
Seebeck coefficient α (μV K^{-1})	24	118
Power factor $\sigma\alpha^2$ (μW K^{-2} m^{-1})	0.5	6.3
Hall coefficient R_H (m^3 K^{-1})	1.4×10^{-2}	1.8×10^{-2}
Fermi level E_f (eV)	−0.72	−0.70
Scattering parameter λ	1.13	2.99
Carrier concentration n (cm^{-3})	1.3×10^{20}	0.9×10^{20}
Carrier mobility μ (cm^2 V^{-1} s^{-1})	0.45	0.31

The P3HT–Bi_2Te_3 interfacial band diagram is illustrated in Fig. 5. As a degenerate semiconductor, the Fermi level of Bi_2Te_3 is positioned inside the valence band. The band gap E_g and work function Φ of Bi_2Te_3 nanowires are taken from its bulk values.[26,29] For P3HT, as a non-degenerate semiconductor,[47] the Fermi level is positioned nearly at the centre of the energy gap between the LUMO and HOMO.[30] In addition, because the work function of Bi_2Te_3 (*i.e.*, $\Phi = \sim 5.3$ eV) is larger than that of P3HT (*i.e.*, $\Phi = \sim 4.1$ eV),[27,48] the upward band bending at the P3HT–Bi_2Te_3 interface may partially eliminate the interfacial barrier to facilitate the charge carrier transfer.[13] The positive sign of the Seebeck coefficients in both P3HT and P3HT–Bi_2Te_3 (Fig. 4a) was related to the p-type character of the semiconductor. Therefore, the transport characteristics of charge carriers (*i.e.*, holes) across the P3HT–Bi_2Te_3 interface are probably determined by the height of the potential barrier between the HOMO level of P3HT and the valance-band level of Bi_2Te_3.[28]

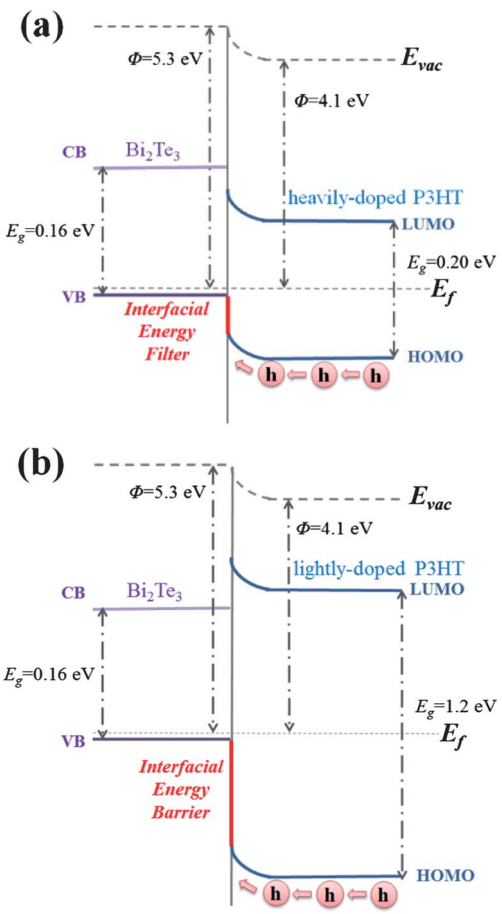

Fig. 5 The band diagram of the P3HT–Bi_2Te_3 interface: (a) the nanocomposite based on the heavily doped P3HT matrix; (b) the nanocomposite based on the lightly doped P3HT matrix.

According to theoretical predictions, an effective barrier height for energy filtering in combination with a high electrical conductivity lies in the range of 0.04–0.10 eV, for a composite of two materials having very similar band gaps to form a heterojunction structure, which can be highly advantageous for thermoelectric applications due to an expected increase in the power factor.[49] For the nanocomposite discussed above (Table 1), which was composed of the heavily doped P3HT matrix and 20 wt% Bi_2Te_3 nanowires, the band gap of bulk Bi_2Te_3 is 0.16 eV, and the band gap of the heavily doped P3HT is probably below 0.20 eV.[30,43] An interfacial potential barrier of below 0.10 eV forms at the P3HT–Bi_2Te_3 interface (Fig. 5a) to selectively scatter low-energy carriers rather than high-energy carriers, which is correlated well with the optimized barrier height of below 0.10 eV when combining two materials with very similar band gaps for an effective energy filtering.[13,49,50] For the nanocomposite based on the lightly doped P3HT matrix (*i.e.*, $\sigma < 200$ S m^{-1}, Fig. 4 and Fig. S3†), the band gap of P3HT extends to be larger than 0.2 eV (*e.g.*, 1.2 eV in Fig. 5b),[30] no longer comparable to that of Bi_2Te_3, and the interfacial potential barrier of P3HT–Bi_2Te_3 also increases. Consequently, most charge carriers will be strongly scattered by the potential barrier leading to reduced carrier transfer and electrical conductivity, which is likely responsible for the observation of the reduced Seebeck coefficient and power factor in the nanocomposites produced from lightly doped P3HT matrix (Fig. 4a inset). The P3HT–Bi_2Te_3 interfaces in the lightly doped system probably act as an energy barrier without the energy-filtering effect due to the large potential barrier and incompatible band gaps of P3HT–Bi_2Te_3 nanocomposites. It is noteworthy that precise measurement of the work function and the band gap of P3HT–Bi_2Te_3 nanocomposites as a function of doping and nanowire concentration is helpful to better illustrate the energy-filtering effect at organic–inorganic semiconductor interfaces, which will be explored in our future work. Even though the increased scattering parameter provides evidence of the fact that the low-energy carriers are more strongly scattered than the high-energy carriers leading to the enhanced power factor, it still needs further experimental proofs, especially the direct measurement of the energy-dependent scattering rate, to solidify the energy-filtering effect in P3HT–Bi_2Te_3 nanocomposites.[14] In this context, alternative explanations and models (*e.g.*, a series connected composite model) may also be suitable to describe the thermoelectric data in this work. Additionally, several approaches may also lead to the enhancement of the Seebeck coefficient in thermoelectric nanocomposites, such as inducing impurity-scattering centres, creating resonance impurity levels inside the valence band, and fabricating series-connected thermoelectric composites.[3,14] Moreover, the oxidization layer outside the Bi_2Te_3 nanowires may form an additional interfacial barrier to affect the charge transfer in P3HT–Bi_2Te_3 nanocomposites, which will make the band diagram more complex, and the possible effect of Bi_2Te_3 oxidation on the thermoelectric behaviour is also worthy to be explored.

4. Conclusion

In conclusion, we have demonstrated a viable method to enhance the Seebeck coefficient and power factor of the conducting polymer P3HT by mixing with Bi_2Te_3 nanowires to substantially scatter low-energy carriers *via* the energy-filtering effect at the P3HT–Bi_2Te_3 interface. The resulting P3HT–Bi_2Te_3 nanocomposites exhibited a several-fold increase in the Seebeck coefficient without greatly suppressing the electrical conductivity, thereby leading to a high power factor of 13.6 μW K^{-2} m^{-1} at room temperature compared to that of 3.9 μW K^{-2} m^{-1} in P3HT. The transport characteristics of P3HT–Bi_2Te_3 nanocomposites, including the carrier concentration, mobility, and energy-dependent scattering parameter, could be derived from the experimentally measured electrical conductivity, Seebeck coefficient, and Hall coefficient. The improved thermoelectric performance was attributed to a possible energy-filtering effect at the P3HT–Bi_2Te_3 interface, where low-energy carriers were scattered more strongly than high-energy carriers by the appropriately engineered interfacial barrier, thereby yielding the significantly increased Seebeck coefficient and power factor. The strategy of largely improving the power factor *via* rationally engineering the organic–inorganic semiconductor interface of polymer nanocomposites may stand out as a promising route to high-performance, large-area, and flexible polymer TE materials.

Acknowledgements

We gratefully acknowledge Dr G.T. Lee at Ecopia Corporation, Gyeonggi-do, South Korea for the measurement of Hall coefficients. We also gratefully acknowledge the support from the National High Technology Research and Development Program of China (grant no. 2008AA032101) and Natural Science Foundation of China (grant no. 20990231). Z.L. gratefully acknowledges the support from the Georgia Institute of Technology.

Notes and references

1 F. J. DiSalvo, *Science*, 1999, **285**, 703.
2 D. Vashaee and A. Shakouri, *Phys. Rev. Lett.*, 2004, **92**, 106103.
3 M. S. Dresselhaus, G. Chen, M. Y. Tang, R. G. Yang, H. Lee, D. Z. Wang, Z. F. Ren, J. P. Fleurial and P. Gogna, *Adv. Mater.*, 2007, **19**, 1043.
4 R. Venkatasubramanian, E. Siivola, T. Colpitts and B. O'Quinn, *Nature*, 2001, **413**, 597.
5 K. F. Hsu, S. Loo, F. Guo, W. Chen, J. S. Dyck, C. Uher, T. Hogan, E. K. Polychroniadis and M. G. Kanatzidis, *Science*, 2004, **303**, 818.
6 W. J. Xie, J. He, H. J. Kang, X. F. Tang, S. Zhu, M. Laver, S. Y. Wang, J. R. D. Copley, C. M. Brown, Q. J. Zhang and T. M. Tritt, *Nano Lett.*, 2010, **10**, 3283.
7 S. V. Faleev and F. Leonard, *Phys. Rev. B: Condens. Matter Mater. Phys.*, 2008, **77**, 214304.
8 D. K. Ko, Y. J. Kang and C. B. Murray, *Nano Lett.*, 2011, **11**, 2841.
9 J. S. Son, M. K. Choi, M. Han, K. Park, J. Kim, S. J. Lim, M. Oh, Y. Kuk, C. Park, S. Kim and T. Hyeon, *Nano Lett.*, 2012, **12**, 640.
10 C. Yu, Y. S. Kim, D. Kim and J. C. Grunlan, *Nano Lett.*, 2008, **8**, 4428.
11 C. Z. Meng, C. H. Liu and S. S. Fan, *Adv. Mater.*, 2010, **22**, 535.
12 K. C. See, J. P. Feser, C. E. Chen, A. Majumdar, J. J. Urban and R. A. Segalman, *Nano Lett.*, 2010, **10**, 4664.
13 Y. C. Zhang, M. L. Snedaker, C. S. Birkel, X. L. Ji, Y. F. Shi, D. Liu, X. N. Liu, M. M. Moskovits and G. D. Stucky, *Nano Lett.*, 2012, **12**, 1075.
14 M. Zebarjadi, K. Esfarjani, M. S. Dresselhaus, Z. F. Ren and G. Chen, *Energy Environ. Sci.*, 2012, **5**, 5147.
15 N. Dubey and M. Leclerc, *J. Polym. Sci., Part B: Polym. Phys.*, 2011, **49**, 467.
16 M. He, F. Qiu and Z. Q. Lin, *J. Mater. Chem.*, 2011, **21**, 17039.
17 Z. L. Wang, *Adv. Mater.*, 2012, **24**, 280.

18 M. He, W. Han, J. Ge, Y. L. Yang, F. Qiu and Z. Q. Lin, *Energy Environ. Sci.*, 2011, **4**, 2894.
19 M. He, W. Han, J. Ge, W. J. Yu, Y. L. Yang, F. Qiu and Z. Q. Lin, *Nanoscale*, 2011, **3**, 3159.
20 M. He, L. Zhao, J. Wang, W. Han, Y. L. Yang, F. Qiu and Z. Q. Lin, *ACS Nano*, 2010, **4**, 3241.
21 M. He, J. Ge, M. Fang, F. Qiu and Y. L. Yang, *Polymer*, 2010, **51**, 2236.
22 J. Ge, M. He, F. Qiu and Y. L. Yang, *Macromolecules*, 2010, **43**, 6422.
23 R. D. McCullough, *Adv. Mater.*, 1998, **10**, 93.
24 A. J. Heeger, *Angew. Chem., Int. Ed.*, 2001, **40**, 2591.
25 X. A. Yan, B. Poudel, Y. Ma, W. S. Liu, G. Joshi, H. Wang, Y. C. Lan, D. Z. Wang, G. Chen and Z. F. Ren, *Nano Lett.*, 2010, **10**, 3373.
26 D. Haneman, *Phys. Rev.*, 1960, **119**, 567.
27 S. Sapp, S. Luebben, Y. B. Losovyj, P. Jeppson, D. L. Schulz and A. N. Caruso, *Appl. Phys. Lett.*, 2006, **88**, 152107.
28 D. Y. Godovski, *Thermal and Electrical Conductivity of Polymer Materials*, Springer-verlag, Berlin, 1995.
29 T. C. Harman, B. Paris, S. E. Miller and H. L. Goering, *J. Phys. Chem. Solids*, 1957, **2**, 181.
30 P. Chaudhury and S. P. Bhattacharyya, *Int. J. Quantum Chem.*, 2003, **91**, 663.
31 B. Mayers and Y. N. Xia, *J. Mater. Chem.*, 2002, **12**, 1875.
32 J. Guo, X. Wang and T. Wang, *J. Appl. Phys.*, 2007, **101**, 063537.
33 M. Chirea, A. Freitas, B. S. Vasile, C. Ghitulica, C. M. Pereira and F. Silva, *Langmuir*, 2011, **27**, 3906.
34 Y. W. Koh, C. S. Lai, A. Y. Du, E. R. T. Tiekink and K. P. Loh, *Chem. Mater.*, 2003, **15**, 4544.
35 J. J. Kim, S. H. Kim, S. W. Suh, D. U. Choe, B. K. Park, J. R. Lee and Y. S. Lee, *J. Cryst. Growth*, 2010, **312**, 3410.
36 A. L. Prieto, M. S. Sander, M. Martin-Gonzalez, R. Gronsky, T. Sands and A. M. Stacy, *J. Am. Chem. Soc.*, 2001, **123**, 7160.
37 L. Zhao, X. C. Pang, R. Adhikary, J. W. Petrich, M. Jeffries-EL and Z. Q. Lin, *Adv. Mater.*, 2011, **23**, 2844.
38 J. Sun, M. L. Yeh, B. J. Jung, B. Zhang, J. Feser, A. Majumdar and H. E. Katz, *Macromolecules*, 2010, **43**, 2897.
39 M. S. Jeng, R. G. Yang, D. Song and G. Chen, *J. Heat Transfer*, 2008, **130**, 042410.
40 Y. Xuan, X. Liu, S. Desbief, P. Leclere, M. Fahlman, R. Lazzaroni, M. Berggren, J. Cornil, D. Emin and X. Crispin, *Phys. Rev. B: Condens. Matter Mater. Phys.*, 2010, **82**, 115454.
41 G. Chen and A. Shakouri, *J. Heat Transfer*, 2002, **124**, 242.
42 N. Colaneri, M. Nowak, D. Spiegel, S. Hotta and A. J. Heeger, *Phys. Rev. B: Condens. Matter Mater. Phys.*, 1987, **36**, 7964.
43 D. Giri and K. Kundu, *Phys. Rev. B: Condens. Matter Mater. Phys.*, 1996, **53**, 4340.
44 K. H. Lee, R. Menon, C. O. Yoon and A. J. Heeger, *Phys. Rev. B: Condens. Matter Mater. Phys.*, 1995, **52**, 4779.
45 T. Unuma, K. Fujii, H. Kishida and A. Nakamura, *Appl. Phys. Lett.*, 2010, **97**, 033308.
46 M. Logdlund, R. Lazzaroni, S. Stafstrom, W. R. Salaneck and J. L. Bredas, *Phys. Rev. Lett.*, 1989, **63**, 1841.
47 T. C. Chung, J. H. Kaufman, A. J. Heeger and F. Wudl, *Phys. Rev. B: Condens. Matter Mater. Phys.*, 1984, **30**, 702.
48 D. Haneman, *J. Phys. Chem. Solids*, 1959, **11**, 205.
49 M. Scheele, N. Oeschler, I. Veremchuk, S. O. Peters, A. Littig, A. Kornowski, C. Klinke and H. Weller, *ACS Nano*, 2011, **5**, 8541.
50 S. Sumithra, N. J. Takas, D. K. Misra, W. M. Nolting, P. F. P. Poudeu and K. L. Stokes, *Adv. Energy Mater.*, 2011, **1**, 1141.

